LAWRENCE
LIVERMORE
NATIONAL
LABORATORY

LLNL-TR-849902

Ground Motion Models (GMMs) Improvements Using Earthquake Simulations on High Performance Computers

A. Pitarka, A. Rodgers, A. Aguiar, V. Graizer

June 5, 2023

Disclaimer

This work performed under the auspices of the U.S. Department of Energy by Lawrence Livermore National Laboratory under Contract DE-AC52-07NA27344.

Ground Motion Models (GMMs) Improvements Using Earthquake Simulations on High Performance Computers

[1]Arben Pitarka, [1]Artie Rodgers, [1]Ana Aguiar, and [2]Vladimir Graizer

Lawrence Livermore National Laboratory, Livermore CA

[2]US Nuclear Regulatory Commission, Washington DC

1.0 EXECUTIVE SUMMARY

A computationally efficient simulation platform was developed that can provide representative synthetic ground motions from crustal earthquakes in the Stable Continental Regions of Central and Eastern US (CEUS), using 3D modeling and high-performance computing. The main objective was to use synthetic ground motion to provide constrains to refinements of exiting ergodic Ground Motion Models (GMMs), for large magnitude earthquakes and near-fault distances, for which these models are less reliable. Physics-based broadband (0-5Hz) ground motion simulations were used to estimate the near-fault ground motion amplitudes and within event and between-event variabilities associated with fault rupture characteristics.

As part of a strategy for selecting a reginal velocity model and validation of developed rupture modeling technique, ground motions from the moment magnitude *Mw*5.0 November 7, 2016 Cushing Oklahoma (Taylor et al., 2017), and *Mw*5.8 September 3, 2016 Pawnee Oklahoma earthquakes were simulated. In our simulations we used a 3D regional velocity model that was based on Saikia's 1D velocity model (1994). Saikia's model demonstrated better performance in modelling high frequency regional wave propagation for CEUS region. The proposed 3D model includes lateral variations added to the 1D background model using the stochastic scheme of Pitarka and Mellors (2021). Comparisons of the simulations with recordings of both earthquakes demonstrated the reliability of our deterministic simulation approach while emphasizing the importance of including small-scale variability in the regional velocity model needed to reproduce the observed high-frequency wave scattering effects.

As part of validation analysis, comparisons with different GMMs for a *Mw*6.5 earthquake in the CESUS region resulted in a very good match between the simulated and empirical ground motion models.

Initial investigations of within-event and between-event ground motion variabilities for *Mw*6.5 scenario earthquakes on a strike-slip fault, suggest that they are strongly related to spatial slip and slip rate variations, average rupture velocity, rupture area and rupture initiation location. For certain scenarios we found that the ground motion variability observed at near-fault distances (< 5 km) also persists at longer distances. Regardless of the rupture scenario, the simulated ground motion tends to fully saturate at short distances and for all periods. The near-fault saturation has to do with the attenuation of waves propagating along the fault and local rupture radiation pattern that also contribute to stronger ground motion variation at such distances. Analysis of effects of rupture initiation location suggest that the peak ground motion (PGV) and spectral acceleration (SA) can be quite variable due to rupture directivity effects. Such effects are stronger at periods longer than 1s.

The effect of the 1D velocity models and surface topography on simulated ground motion were investigated by comparing three component synthetic seismograms computed at selected sites. Effect of surface topography was considered using the ratio between spectral accelerations simulated for two 1D models with flat surface topography and realistic model with surface topography. Overall, the topography slightly amplifies (by ~30%) the ground motion amplitude in the frequency range 1-3Hz. The effect of topography is more visible in the surface and coda waves portion of the seismograms.

1.0 INTRODUCTION

This collaborative study between the LLNL and NRC aims at testing a high-performance computing simulation platform for ground motion simulations that will be used to develop physical constrains needed to guide improvements of Ground Motion Models (GMMs) for crustal earthquakes at short distances and large magnitudes. The Seismology Group at the LLNL has developed a physics-based earthquake rupture model generator and computationally efficient methods for earthquake ground motion simulations. The LLNL simulation technique allows for regional-scale wave propagation modelling in highly heterogenous media with realistic surface topography enabled by the curvilinear mesh finite-difference formulation with grid refinements adopted by the SW4. SW4 is a wave propagation modelling computer program developed at the LLNL that can be obtained through the Computational Infrastructure for Geodynamics website specialized in validated computer programs for geophysics (https://geodynamics.org/cig/software/sw4/). The Graves and Pitarka (GP) (Graves and Pitarka, 2016) physics-based earthquake rupture generator adopted in the platform has been validated against recorded ground motions from recent earthquakes in California and Japan (e.g., Pitarka et al.,2022; Pitarka e al, 2017; Rodgers et al., 2019,2020). It allows for deterministic ground motion simulations in the frequency range 0–10 Hz which is critical in the evaluation of NPP structures.

The main objective of this project is to provide technical capabilities for producing physics-based ground motion that can be used to constrain the GMMs for Stable Continental Regions (SCR) and Active Crustal Regions (ACR) at short distances and large magnitudes. Here we performed a feasibility study for *Mw*6.5 strike slip scenario earthquakes simulated using our Broad-Band Simulation Platform customized for earthquakes in the US Stable Continental Region.

We started by investigating the performance of the simulation platform in ground motion simulations for two local earthquakes in central US, and in synthetic ground motion comparisons with GMMs developed for Central Eastern US (CEUS). The synthetics were later used to analyse potential ground motion saturation at near-fault distances. Through multiple realizations of the earthquake rupture the scenario-based simulations were

designed to investigate the ground motion variability due to different rupture model parameters, including slip distribution, peak slip rate, rupture velocity, rupture area and hypocenter location. The unknown range of these parameters is the source of uncertainties in probabilistic and deterministic seismic hazard assessment. Special attention was placed on the investigation of rupture directivity effects on near-fault ground motion, and effects of surface topography. Our study is intended to help the development of a technical bases for research supporting updates to ground motion models currently being used by the applicants and licenses, as well as updates to the Regulatory Guide 1.208.

2.0 GROUND MOTION SIMULATION OF *Mw*6.5 SCENARIO EARTHQUAKES ON A STRIKE SLIP VERTICAL FAULT

The simulations of *Mw*6.5 scenario earthquakes were performed in the frequency range 0-5 Hz using a 3D reginal model, covering an area of 90km x 110km, with depth extending to 40 km, with modest surface topography from western North Carolina (shown in Figure 1). We used a curvilinear mesh with depth dependent refinements to model the surface topography, and a 3D regional velocity model with a minimum grid spacing of 25m that ensures a numerical accuracy up to the target frequency of 5Hz for a min Vs = 1000m/s. The ground motion time histories are computed on a dense grid of stations with a 2 km grid spacing. The stations spacing is reduced to 1km at fault distances smaller than 5 km. The 3D velocity model is designed to capture wave propagation effects on hard rock, including overall low attenuation that is typical for CEUS regions. The high frequency wave scattering effect is modelled by including small-scale structural variations in the velocity model. The small-scale variations are introduced by correlated random perturbations of the velocity, generated with the vonKarman model as proposed by Pitarka and Mellors (2021). Figure 2 illustrates the small-scale variation in shallow sedimentary layers generated with our stochastic modelling scheme. The parameters of stochastic velocity perturbations are applied in the depth range 0-7km. Their depth dependent variation is shown in Table 1.

Table 1*. Stochastic Velocity Model Parameters used in the vonKarman's stochastic model*

Depth (m)	Lx: horizontal correlation length (m)	Lz: vertical correlation length (m)	sigma	Hurst Number
0-2000	1000	250	0.08	0.1
2-5000	2000	500	0.05	0.4

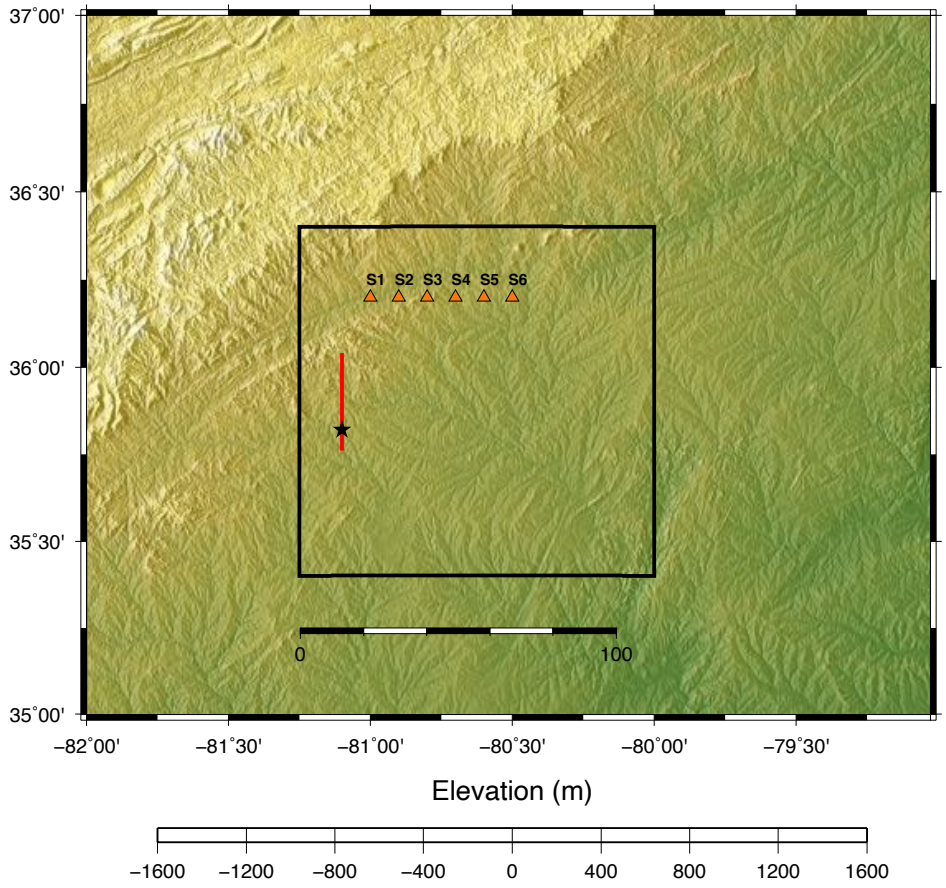

Figure 1. Map of the study area with surface topography. The black rectangle indicates the model location, and the red line indicates the vertical fault trace used in the simulations of M6.5 earthquake on a vertical strike-slip fault. The star indicates the rupture initiation location for the base rupture model, and the red triangles indicate the location of six selected stations used in analysis.

2.1 Kinematic Rupture Models

The kinematc rupture models representing different rupture scenarios were generated with the GP method (Graves and Pitarka, 2016). The GP rupture model is derived from dynamic rupture modelling, and constrained by empirical relationships between the slip and other kinematic rupture parameters such as peak slip rate, rise time, and rupture velocity. The rupture heterogeneity is achieved by correlated random perturbations at different scale lengths. The resulting rupture model incorporates depth-dependent multi-scale spatial variations of slip, slip rate, local faulting mechanism, and rupture velocity, that allow for producing realistic near-fault ground motion on a broad frequency range (Graves and Pitarka,2016; Pitarka et al., 2022). For example, the longer rise time at shallow depths and shorter rise time at greater depths, are designed to represent the depth-dependent frequency content of the generated seismic energy generated by the

fault rupture. We used Somerville at al formula (2021) to calculate the average rise time Tr :

$$Tr = 2.1 * 1.0e\text{-}0.9 * \exp^{(\log(Mo/3))}]$$

and rupture area A:

$$\text{Log}_{10}A = Mw\text{-}4.25$$

developed for Cratonic regions.

Table 2. *Mw6.5 Rupture Scenarios Used in the Simulations*

Group	***Varied Rupture Parameter***	***Number of scenarios***
Group 1	Slip distribution	10
Group 2	Rupture velocity (60%,70%, 80% of Vr)	5
Group 3	Peak slip rate (+/-20%)	3
Group 4	Rupture area (+/-20%)	4
Group 5	Hypocenter location (varies along strike)	6
Group 6	Thrust mechanism	2

In our rupture models we used a planar fault with a length of 26 km, and width of 8 km. The average rupture velocity is set to 82% of the local shear wave velocity in accordance with observed rupture velocity values found for shallow crustal earthquakes on mature faults. Note that the GP assigns small-scale rupture variations that correlate with the local slip, the rupture speed increases in areas where slip is higher and decreases where the slip is lower. The depth to the top of the fault was set to 0.2 km and the dip angle is 90 degrees. The earthquake focal mechanism is assumed to be predominantly of strike-slip type. The average rake angle is set to 0 degree with spatially correlated random perturbations, computed following the GP method.

A suite of 30 rupture models was utilized to capture the inherited ground motion variability from the earthquake rupture. As shown in Table 2 the rupture scenarios were divided in six groups. Within each group we vary a single rupture parameter while keeping the other

rupture parameters fixed. By varying one by one the parameters describing the source, we are able to separate their individual influence on simulated ground motion. Figure 3 illustrates kinematic rupture models with different slip distribution. As part of the parametrical study, we also considered several rupture scenarios with a large slip patch located near the free surface.

a) Shallow Geology

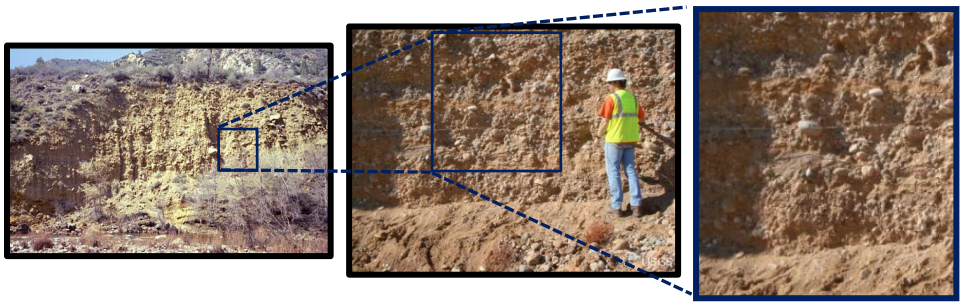

b) Stochastic model of heterogenous stratigraphy

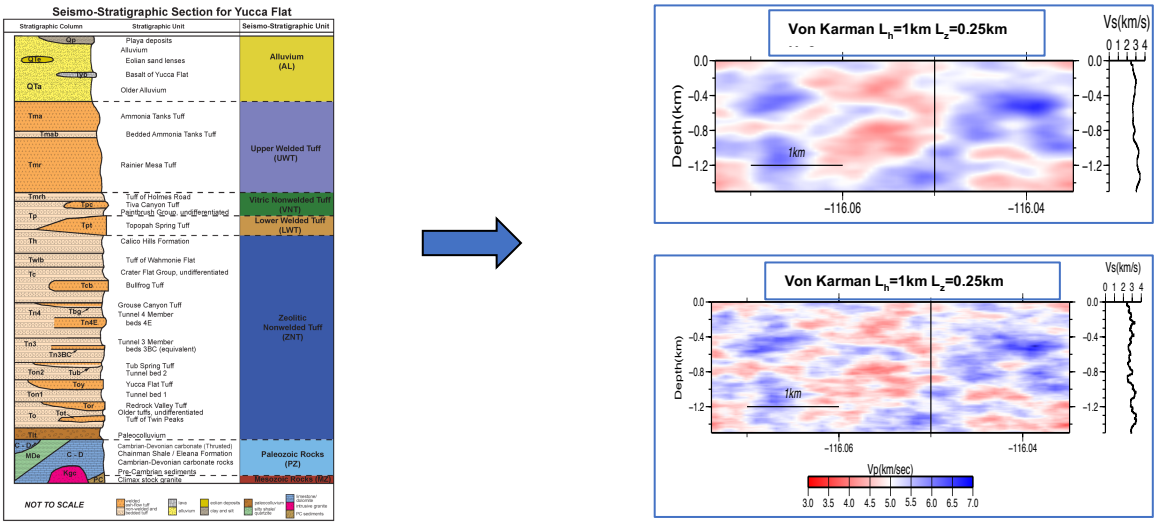

Figure 2. a) Pictures illustrating multiscale variability of the near-surface geology. b) Stochastic velocity models with correlated random perturbations.

2.2 The Regional Velocity Model

In developing a regional 3D velocity model for CEUS, we considered the plane-layered average crustal models of Saikia (1994) and Herman (1995). The 3D velocity model should capture the main characteristics of the shallow crust, including low lateral heterogeneity and low attenuation that is typical for the CEUS region. Near-surface shear wave speeds were kept relatively high at 1000 m/s to represent hard rock site conditions. The two models are shown in Figure 4. They differ from each other in the top 5 km where Sakia's model is characterised by gradual increases of velocity and Q with depth. As it

will be shown below, these small model differences translate into small differences in the simulated ground motion in the considered distance range of 0-80km and frequency range of 0-5Hz.

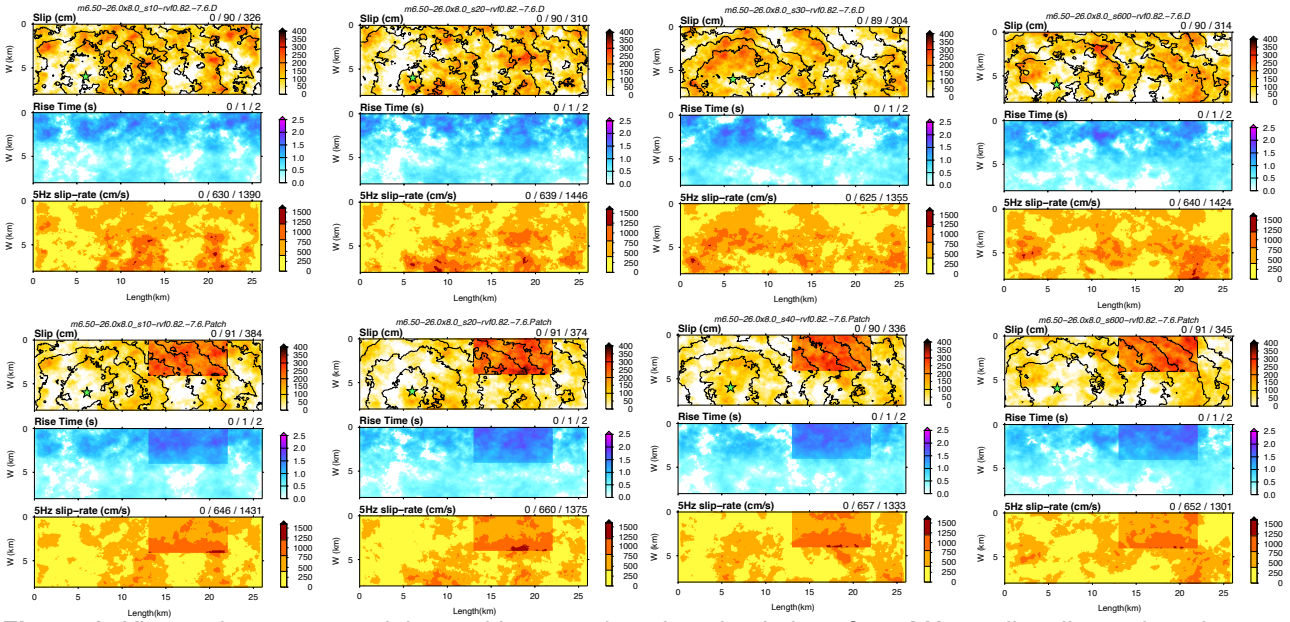

Figure 3. Kinematic rupture models used in ground motion simulations for a M6.5 strike slip earthquakes. In the first four models shown here we varied the slip, and in the four others a large slip patch was added. In each slip model plot the top panel shows the slip distribution and the rupture time indicated by contour lines, the middle panel shows the rise time distribution, and the bottom panel shows the peak slip rate distribution flow-pass filtered at 5Hz.

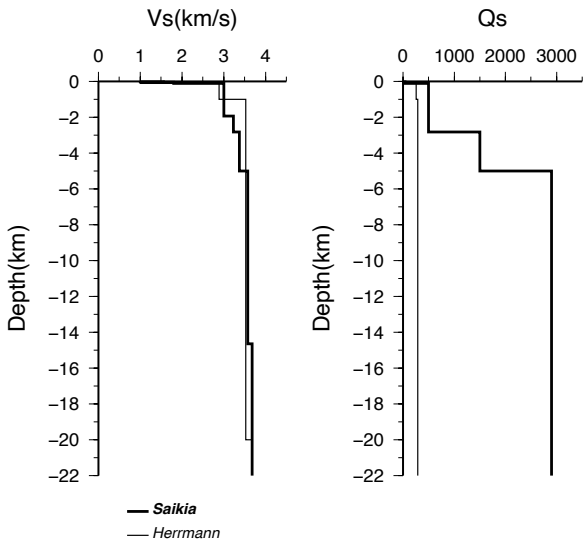

Figure 4. 1D velocity (left panel) and attenuation (right panel) models considered in building a reginal 3D model for the CEUS. Thick line corresponds to the model proposed by Saikia (1994) and thin line corresponds to the model proposed by Herrmann (1995)

We investigated the effect of the 1D velocity models and surface topography on simulated ground motion by comparing three component synthetic seismograms computed at selected sites located north of the fault (see Figure 1). In Figure 5 we compare time histories of three component velocity at three sites. As also seen on the goodness of fit plots between the two models, and between two simulations with and without surface topography, shown in Figure 6 and Figure 7, respectively, Model 2 (Herman's 1D model) generates slightly higher ground motion at frequencies higher than 2Hz. Overall, the topography slightly amplifies (by ~30%) the ground motion amplitude in the frequency range 1-3Hz. The effect of topography is more visible in the surface and coda waves portion of the seismograms. As it will be demonstrated below, because its better performance in modelling high frequency regional wave propagation, we decided to use Saikia's 1D velocity model in building the 3D regional velocity model used in this study. The proposed 3D model also includes lateral variations added to the 1D background model using our stochastic scheme.

3.0 VALIDATIONS OF SIMULATION METHODOLOGY

The performance of the velocity model was analyzed by simulating ground motion recorded during the *Mw*5.0 November 7, 2016 Cushing Oklahoma earthquake (Taylor et al., 2017), and by comparing simulated ground motion with proposed GMMs for the CEUS region for a M6.5 strike slip earthquake.

Table 3. 1D Regional Velocity Model Used in Generating a 3D Velocity Model for CEUS

Depth (m)	Vp (m/s)	Vs(m/s)	Density (g/cm3)	Qp	Qs
30.7	1730	1000	2030	100	50
44.7	2683	1551	2140	100	50
100.0	3119	1803	2276	100	50
1933.0	5190	3000	2611	1000	500
2828	5577	3224	2665	1000	500
5000	5828	3369	2700	3000	1500
14650	6180	3570	2724	5800	2900
25650	6360	3680	2781	5800	2900
33650	7120	4120	3066	5800	2900
36000	7260	4200	3094	5800	2900

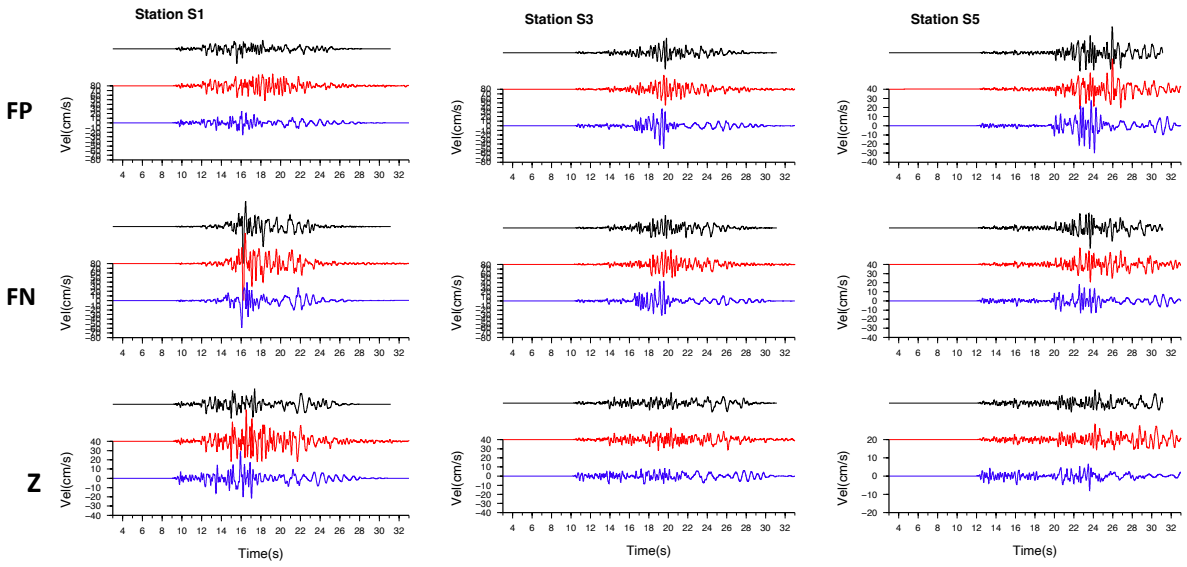

Figure 5. Sensitivity of simulated ground motion to 1D regional velocity models and surface topography effects at station S1, S3, S5. The velocity seismograms are computed with the 1D-Mod1 based on Saikia's 1D velocity model (black traces), the1D-Mod2 based on Herrmann's 1D velocity model (blue traces) and the 1D-Mod1_Topo based on Saikia's 1D velocity model with surface topography (red traces).

3.1 Simulation of the Mw5.0 November 7, 2016 Cushing Oklahoma earthquake

The 2016 Cushing Oklahoma earthquake is one of the few seismic events in the Central US that is well recorded by strong motion stations, mostly in the near field. The stations that recorded the earthquakes are clustered in the epicentral area, with the exception of station 7416 which had an epicentral distance of 72m km (see Figure 8). The ground motion record at 7416 is of poor quality, and it was probably strongly affected by the building response in which it was installed. Figure 9 shows the rupture model used in our simulations. The rupture area A was computed using Somerville's relationship (2021). The comparison of recorded and simulated ground motion using the 3D model with and without correlated random perturbations is shown in Figure10. Overall, despite the arbitrary selection of the rupture model (we did not perform additional simulations to select the rupture model that best fits the data) the simulation reproduced the recorded ground motion characteristics at all near-field stations.

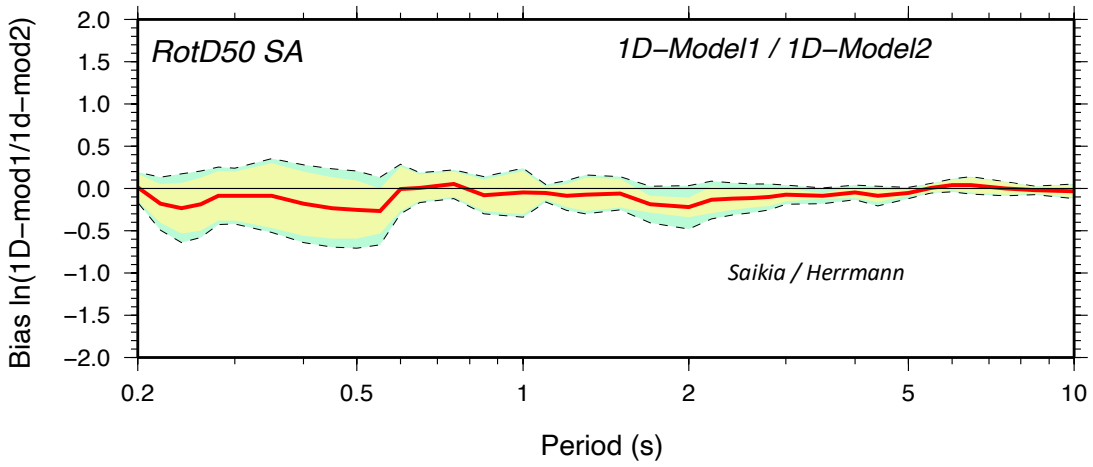

Figure 6. Comparison of 1D velocity models using the ratio between RotD50 SA simulated for the two models, averaged over 6 selected sites shown in Figure 1, in the period range 0.2-10 s. The synthetic ground motions were computed with the 1D-Model1 and 1D-Model2 with flat topography. The red line shows the bias between the two models and the dotted line shows the standard deviation.

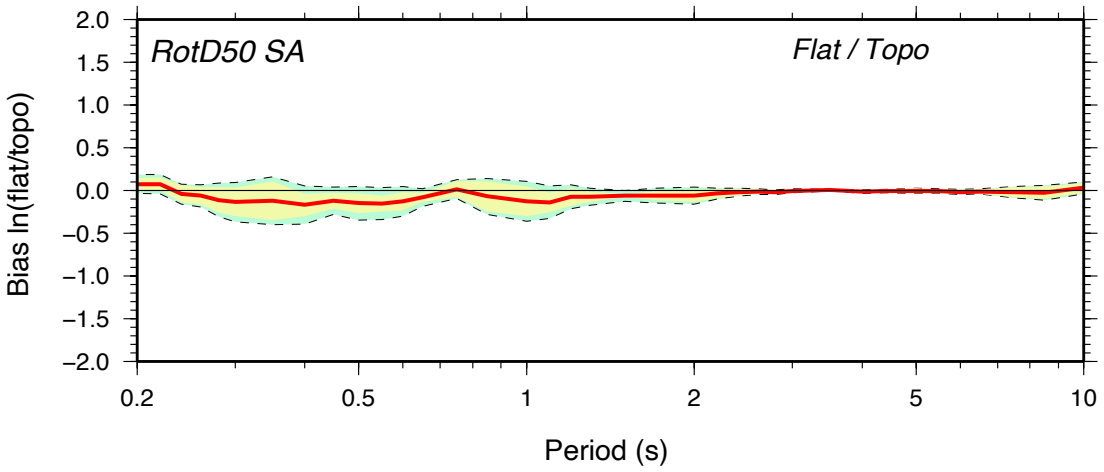

Figure 7. Effect of surface topography using the ratio between RotD50 SA simulated for two 1D models, Model1 with flat surface topography and Model1 with surface topography. The red line shows the bias between the two models and the dotted line shows the standard deviation.

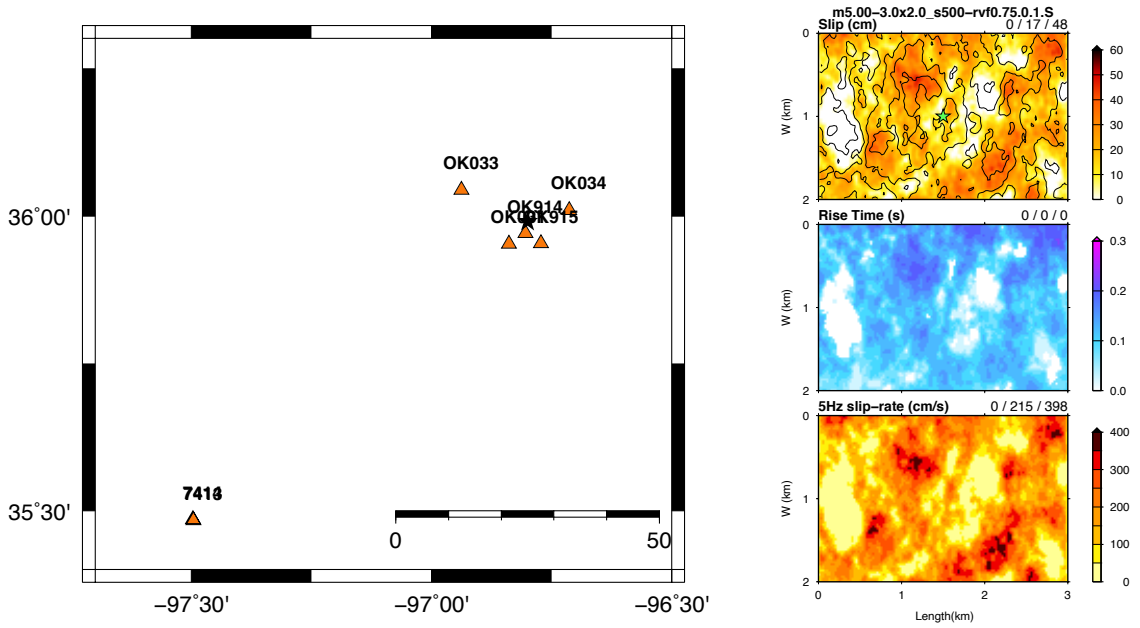

Figure 8. Left Panel: Map of the 3D model area used in the simulation of the *Mw*5.0 November 7, 2016 Cushing Oklahoma earthquake. Black star indicates the epicenter location, and triangles indicate the location of the seismic stations. Right Panel: GP kinematic rupture model of the Cushing Oklahoma earthquake

3.2 Validation against GMMs for the Central-Eastern US

One of the main focused areas of this study is testing the quality of simulations against Ground Motion Models (GMMs). The similarity of our simulations to GMMs builds confidence in our result. In this study we used two GMMs available for Central-Eastern US in comparisons with our simulations:

1. NGA-East (Goulet et al, 2018): This model includes 17 GMMs defined for 24 ground-motion intensity measures, applicable to CENA in the moment magnitude range of 4.0 to 8.2 and covering distances up to 1500 km.
2. G-16v2 model (Graizer,2016): This model is based on the NGA-East horizontal peak ground acceleration database and 5% damped pseudospectral acceleration RotD50 component.

NGA-East model was computed for a VS_{30} = 2800 m/s corrected for VS_{30} =1000 m/s used in our simulations as follows:

From equation (6) in Graizer (2016),

$$\text{Lin Amp} = 1 + \frac{k_{V_{S30}}}{\sqrt{[1-(f_{V_{S30}}/f)]^2 + 1.96(f_{V_{S30}}/f)}}$$

$$k_{V_{S30}} = -0.5\ln(V_{S30}/2800)$$

$$f_{V_{S30}} = V_{S30}/120 - 1.6$$

,

The site correction is shown in Figure10. As demonstrated in Figure 11, it allows for a direct comparison of our simulations with the G16v2 model.

The validation of the simulated ground motion was mainly based on comparisons of computed synthetics with the two empirical GMMs. Figure12 demonstrates the performance of the simulations for four rupture scenarios that are representatives of a series of rupture realizations with different rupture parameters. We then compute the deviation of our simulated data from the models by computing ϵ; a normalized measure of ground motion intensity deviation from the median value predicted by the GMMs. ϵ is the natural log ratio of ground motion intensities (GMI's) normalized by standard deviation:

$$\epsilon = \frac{ln(z) - ln(\hat{z})}{\sigma}$$

z = simulated GMI

$\hat{z}$ = median GMI from the GMM for this event, path, site, etc…

σ = ln standard deviation of $\hat{z}$ (already in ln units)

ϵ of +/-1 means GMI is σ above/below median GMI estimated from the GMM

Small ϵ means the simulated ground motion intensity (GMI) is very similar to the GMI predicted by the GMM. Figure 13 shows the Epsilon variation with the response period. The very low epsilon values obtain for all simulations demonstrate the very good performance of our simulations. The synthetic ground motion has very similar characteristics with the GMMs at all considered periods.

We continued our analysis of the simulation performance by focusing on the comparisons with Graizer's GMM, version G-16v2 (2017). Figure 14 compares Graizer's GMM, for the Rotd50 SA, with ground motion computed for four rupture models with different slip distributions, including one with large slip patch. The simulations performed remarkably well. The synthetic and empirical motions compare extremely well at all periods and distances.

The simulated ground motion is fully saturated at near-fault distances (<10km). This important result is consistent with the saturation constrain adopted in the Grazer's GMM and other models proposed for this region, at all periods, except for the 5s response for which the simulations suggest a slight oversaturation. We will discuss this, as well as its sensitivity to the style of faulting in a subsequent section. These results demonstrate the advantages of using simulated near-fault ground motions to supplement the limited available database of recordings for large earthquakes at small distances.

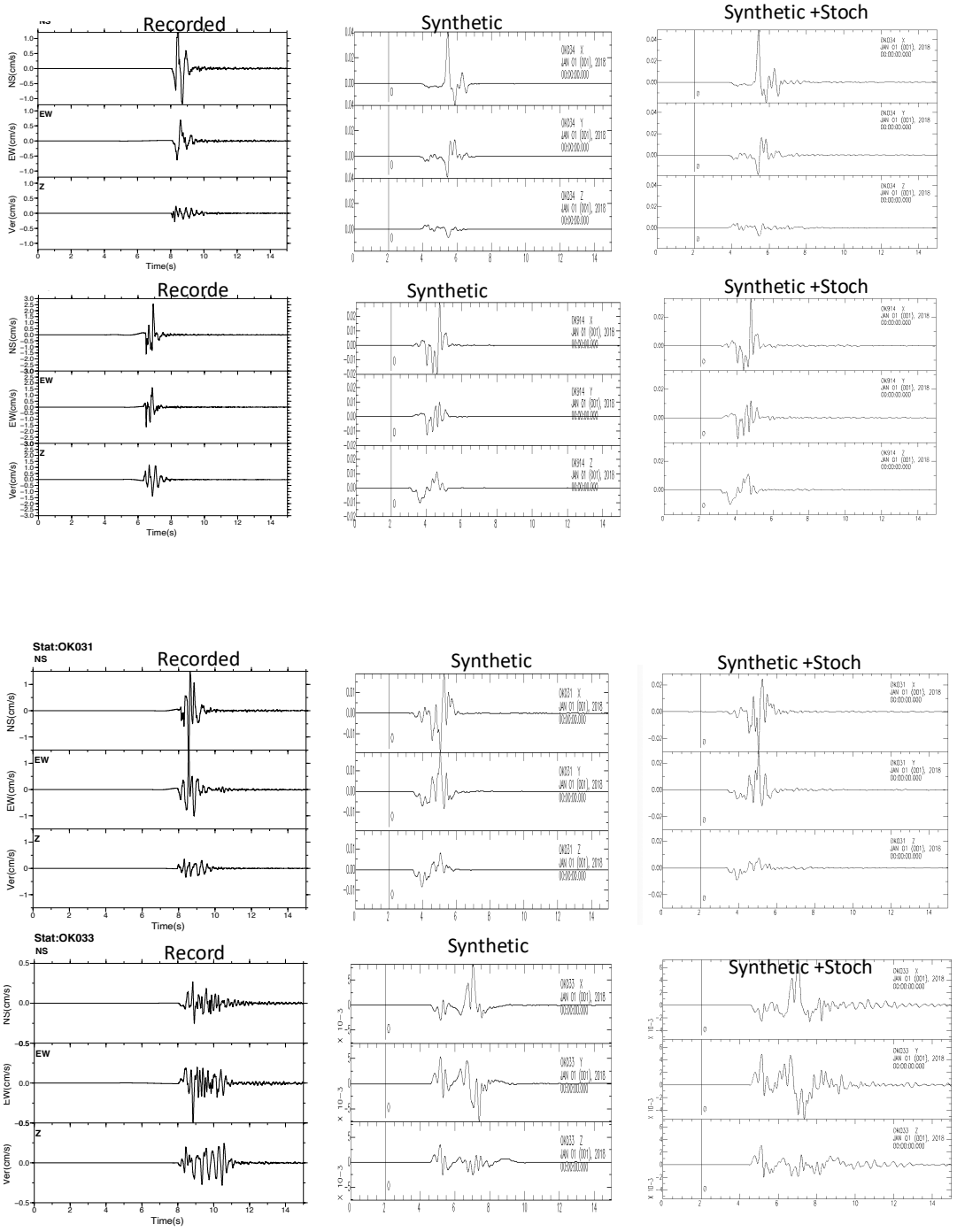

Figure 9. Comparison of recorded (left panels) and synthetic ground motion velocity computed without (middle panels) and with correlated stochastic perturbations (right panels), low-pass filtered at 5Hz.

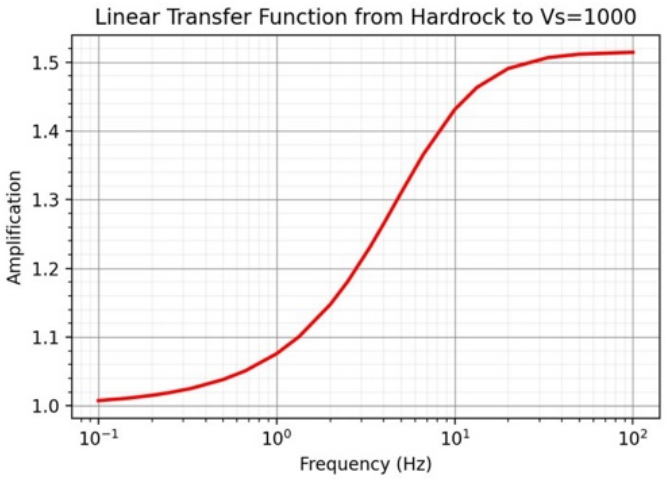

Figure 10. Linear amplification correction curve.

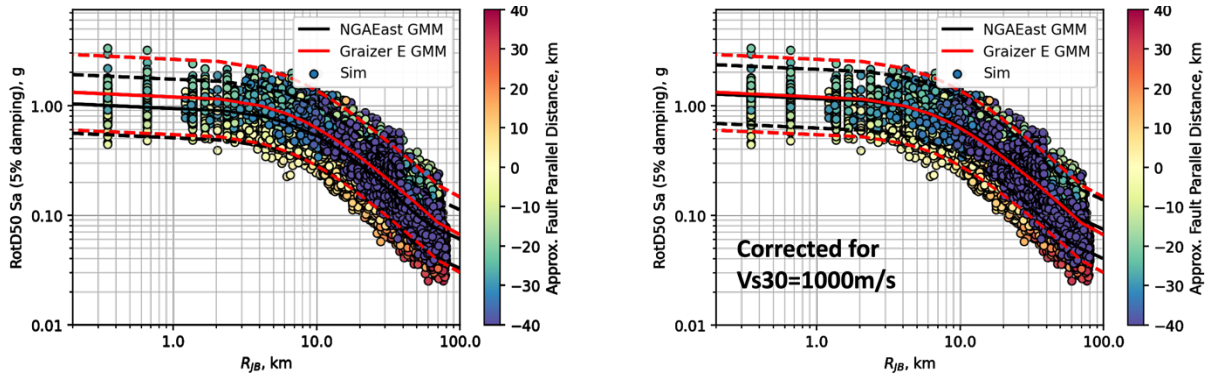

Figure 11. Site Amplification Correction to the base GMM for the Vs30=1000m/s used in the Simulations where NGA-East model is in black and G-16v2 is in red. Left panel shows Graizer's GMM (Graizer, 2016) for Vs =2400m/s and the left pane shows Graizer's model corrected for Vs=1000m/s.

4.0 NEAR-FAULT GROUND MOTION SATURATION AND ITS SENSITIVITY TO RUPTURE KINEMATICS

So far, we have demonstrated that the simulated ground motion and the adopted regional 3D velocity model produce ground motion characteristics that are in line with ground motion predicted by empirical models for M6.5 crustal earthquakes. After gaining confidence in the ability of simulation technique to produce reliable results we used simulations to investigate ground motion characteristics at near-fault distances were the GMMs are poorly constrained. In our investigation we used a series of simulated ground motion produced with a suite of rupture realizations obtained by varying several rupture

parameters within plausible ranges that are known to affect the ground motion. Figure 15 shows examples of rupture models generated by varying rupture speed, peak slip rate, and hypocenter location. As illustrated by the simulated horizontal PGV and PGA maps shown in Figure 16, these rupture scenarios produce ground motion with various strength, both in terms of amplitude and spatial distribution patterns. For example, the rupture model with a shallow slip patch generates stronger ground motion in a region around the large slip area. In contrast, a slip model with an average rupture speed reduced by 25% produces ground motion that is lower compared to that simulated for the base rupture model. Also, different hypocenter locations generate different ground motion amplification patterns that are significant for both PGA and PGV. Finally, two rupture realizations for a vertical thrust fault show lower sensitivity of the horizontal PGA to slip pattern. The high PGA area is concentrated within a narrow belt around the fault trace. In terms of topographic effects, maps of PGA and PGV indicate for a slight increase in amplitude in areas with pronounced surface topography. Our simulations of topographic effects suggest that because of the very high Vs in the shallow layers the surface topography has minor effects.

4.1 Near-Fault Saturation

The near-fault ground motion saturation (0 to 5 km from fault rupture) for moderate and large earthquakes is a subject of current research. Its investigation is hindered by the sparsity of strong motion recordings, especially for large earthquakes with normal and thrust faulting. Despite new strong-motion data recorded from recent earthquakes, there are still not sufficient data that can uniquely prove hypotheses about the behavior of strong- motion attenuation function in the near field used in proposed GMMs (Grazer, 2016). Differences in constrains applied to the near-fault saturation models result in significant differences between empirical near-fault ground motion predictions.This is demonstrated in Figure 17 which compares different GMMs for the SA at 1s for 5.25<M<5.75. The comparison highlights the relative difference between the predicted SA which could be as high as a factor of 2. On the other hand, abundant data for smaller magnitude events clearly show that near-fault ground motion for small magnitude earthquakes does not saturate at short distances. A typical example for an M2.8 earthquake is shown in Figure 17. The recorded data for this earthquake suggest that the ground motion decay with distance is log-scale linear. The controversial hypothesis that a similar pattern may be observed for all magnitude has not found support among many GMMs modeler. Moreover, although very sparse, an increasing number of ground motion records of large earthquakes confirms the saturation hypothesis. Physics-based ground motion simulations using a deterministic approach, as proposed in this study, can be used to guide the extrapolation of observed near-faut ground motion attenuation for small earthquakes to that for intermediate and large earthquakes using simulations. The

numerical modeling can also be used to separate the rupture and wave propagation effects that are significant contributors to the near-fault attenuation for extended sources.

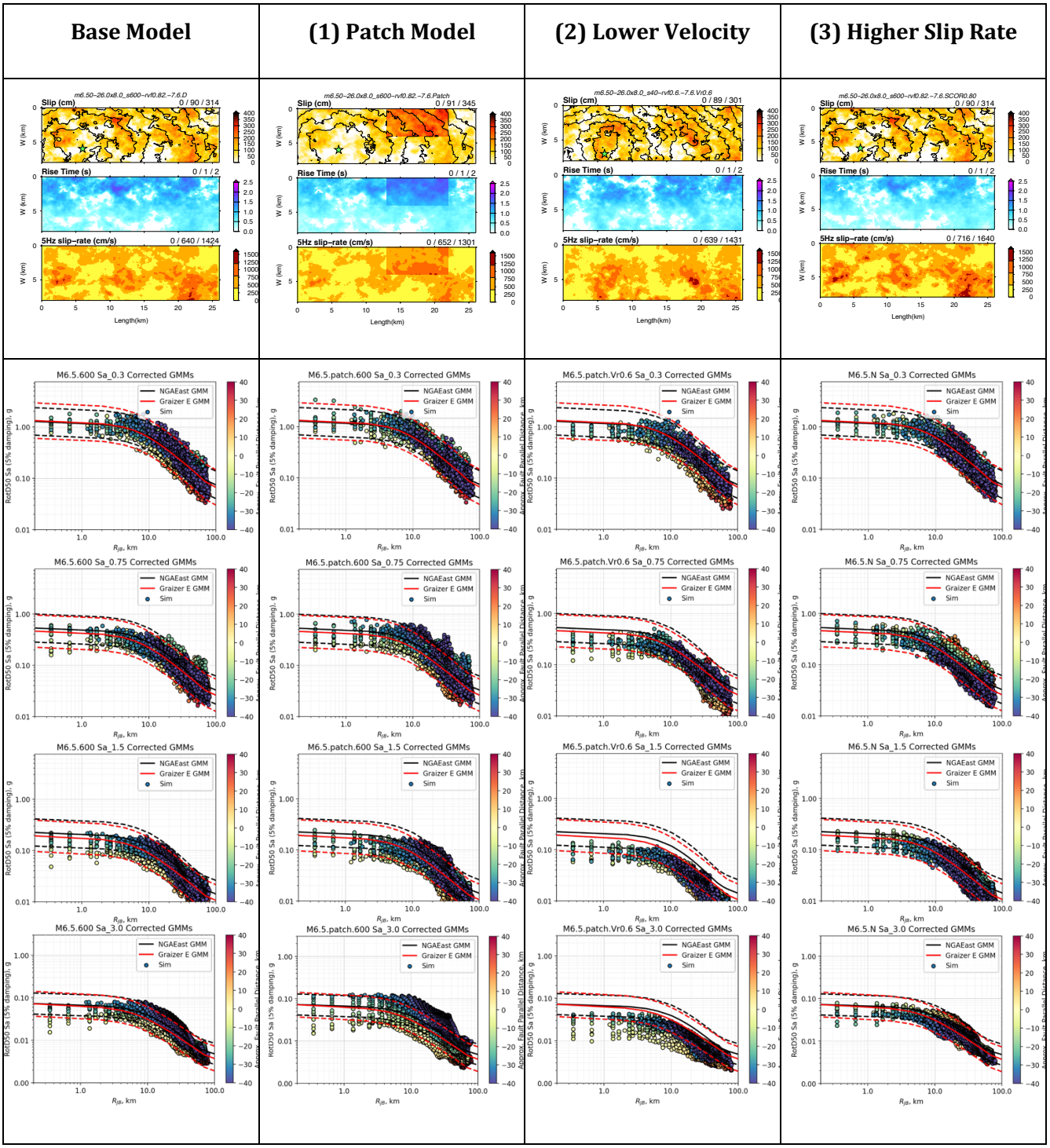

Figure 12. Comparison of simulated RotD50 SA with the NGA-East model (black trace) and G-16v2 (red trace) computed for the base rupture model, rupture model with large slip patch (1), rupture model with lower rupture velocity (2), and rupture model with higher peak slip rate (3). The corresponding rupture models are shown in the upper panels.

Base Model	(1) Patch Model	(2) Lower Velocity	(3) Higher Peak Slip
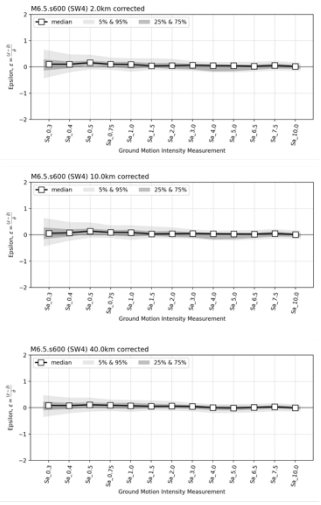	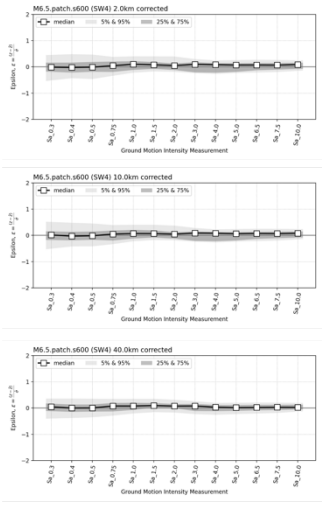	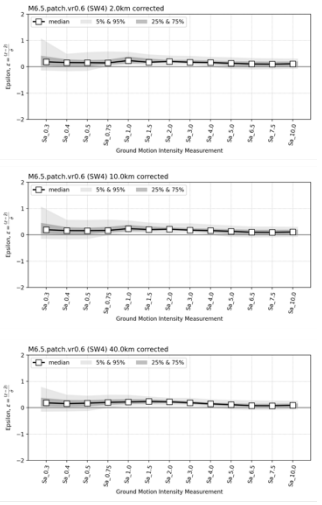	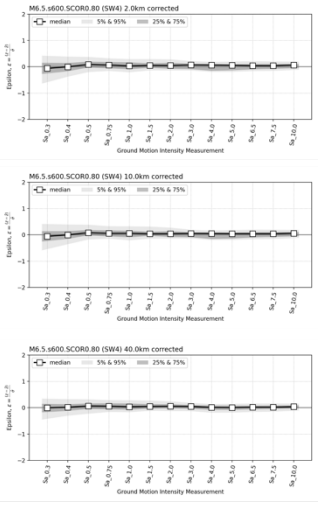

Figure 13. Epsilon values of the base model simulation scenario compared to the epsilon for (1) Scenario for analysing the sensitivity to slip distribution, (2) Scenario for analysing the sensitivity to rupture velocity, and (3) Scenario for analysing roughness of the slip distribution.

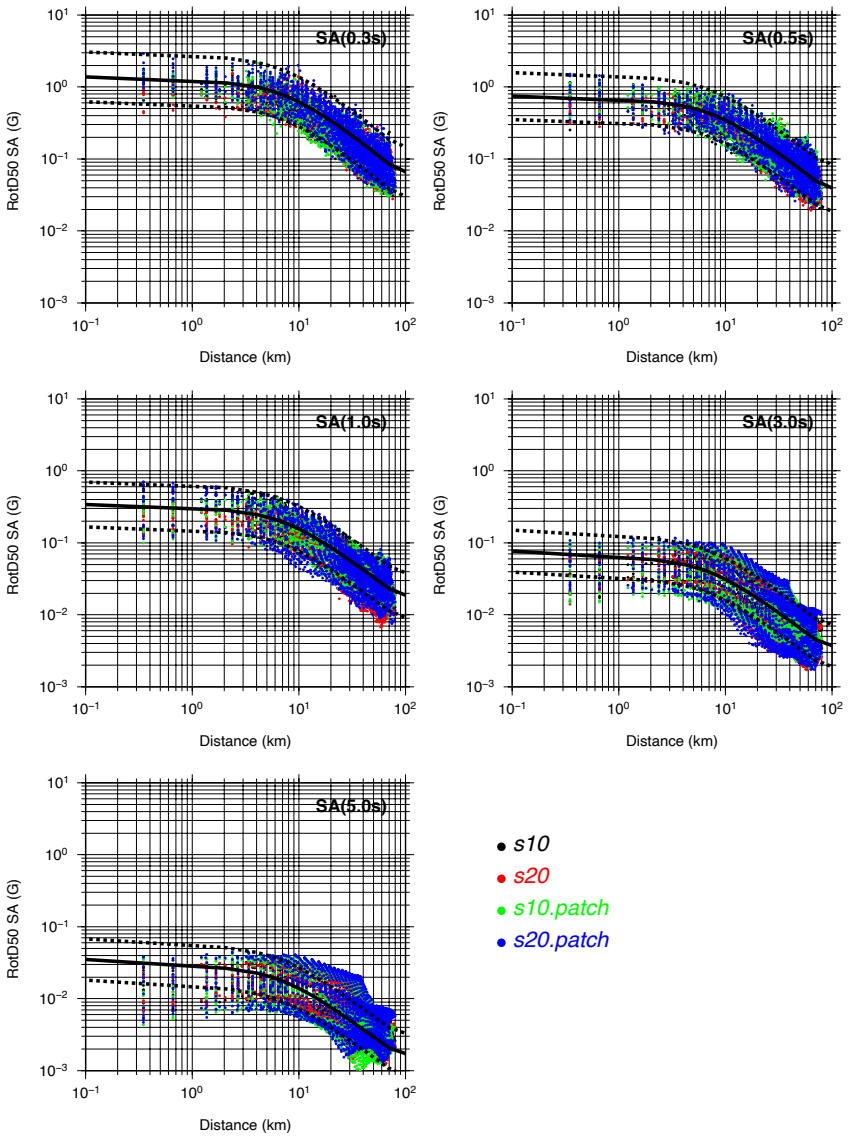

Figure 14. Comparison of Graizer's G-16v2 GMM (2017) (black trace), and computed rotD50 SA,obtained with four different slip distributions indicated by circles with different colours.

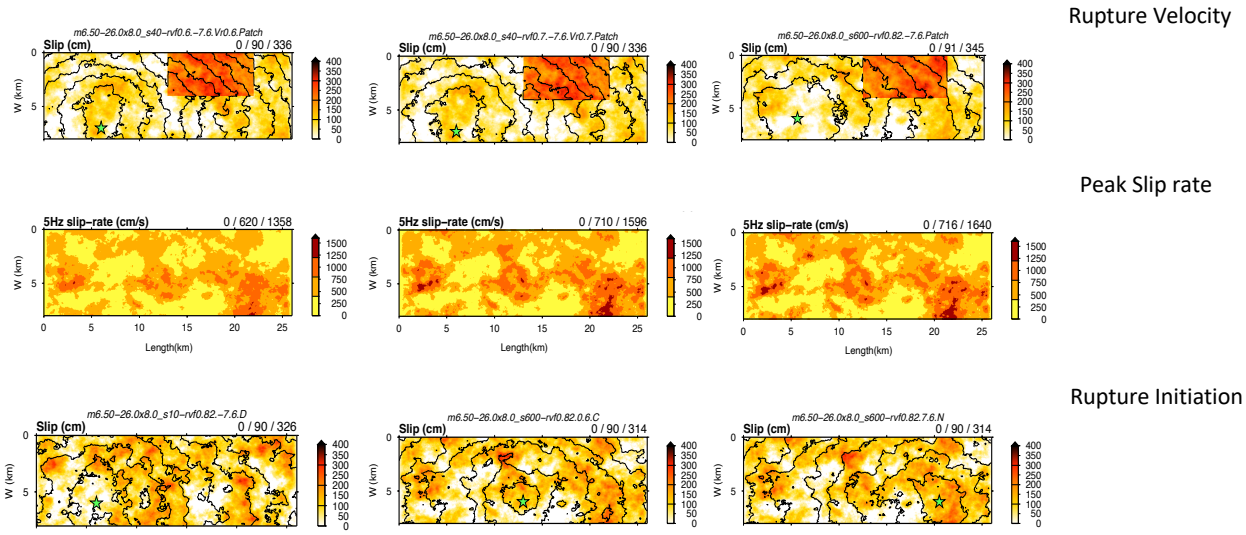

Figure 15. Selected rupture models used in sensitivity analysis of ground motion to rupture parameters including rupture velocity (top panels), peak slip rate (middle panels), and rupture initiation location (bottom panels).

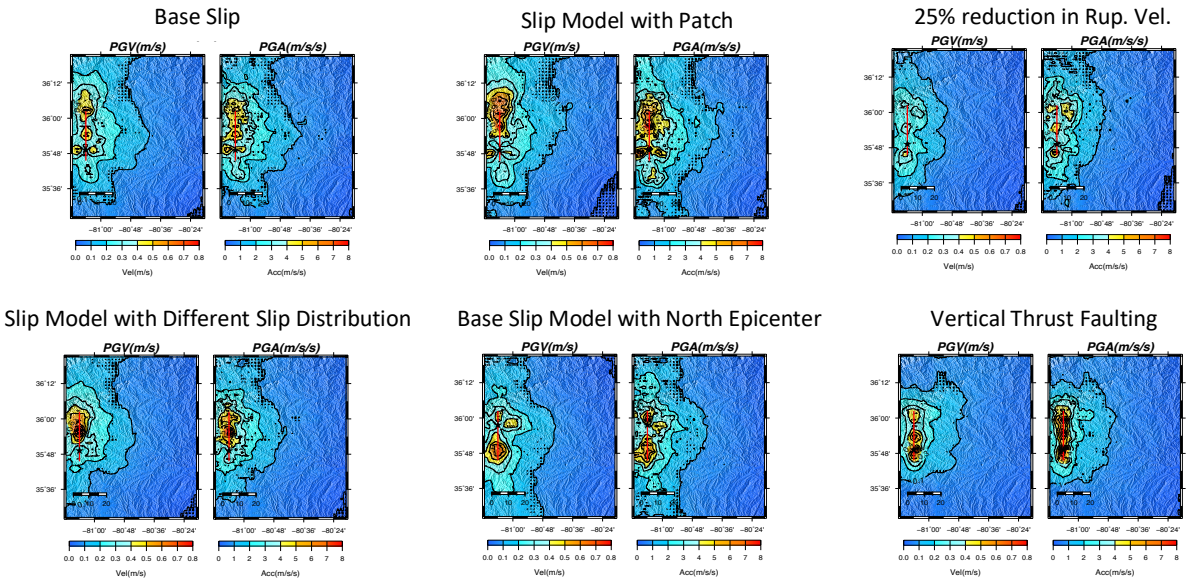

Figure 16. PGV and PGA maps of simulated ground motion using the base slip model, base slip model with one slip patch, a second slip realization, and the base slip model with a northern hypocenter. The fault trace is indicated by the red line and the epicenter is indicated by the black star.

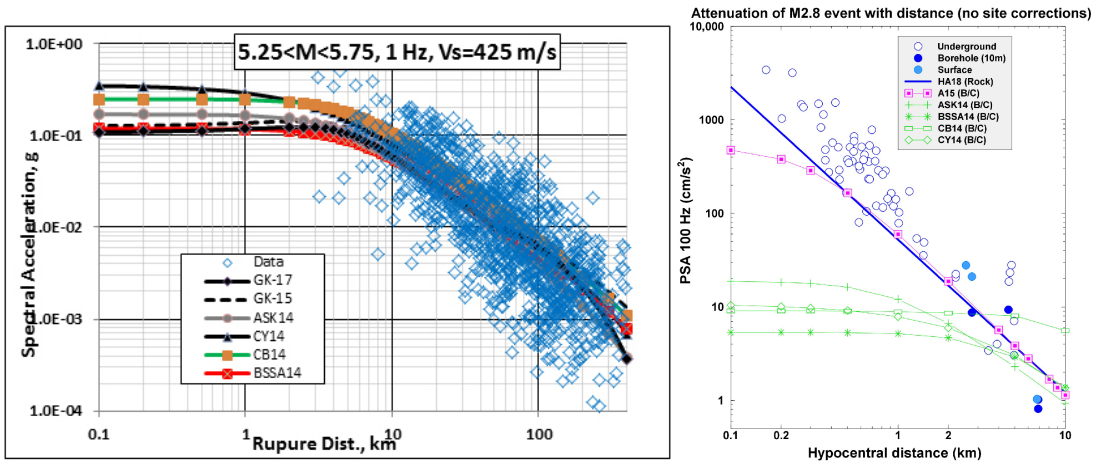

Figure 17. Near-fault ground motion saturation. Left Panel: GMMs for the SA at 1s for 5.25<M<5.75. Rhombs are observed ground motion spectral accelerations. Right Panel: GMMs and recorded PSA for a M2.8 earthquake

We used synthetic ground motions computed for 30 rupture scenarios to investigate the near-fault ground motion saturation for a M6.5 strike-slip earthquake. Figure 18 shows the median ground motion SA at different periods obtained for 10 rupture scenarios for which we only varied the spatial slip distribution. The predicted near fault saturation by Graizer's G-16v2 GMM is very similar to the one produced by our simulations. We note that the simulations produce a slight oversaturation at periods longer than 5s. Using rupture realizations where we only vary one rupture parameter at a time, we investigated the sensitivity of specific rupture characteristics and the near-fault saturation. Plots of RotD50 SA for different groups of rupture scenarios where we varied the fault area, slip rate roughness, and rupture speed are shown in figure 19,20,21. Similar plots of median and +/- one standard deviation of simulated ground motion for several rupture scenarios, including ones with a slip patch, bilateral rupture, reduced rupture area, reduced rupture velocity, higher average slip rate, and thrust faulting are shown in Figures 22 and 23.

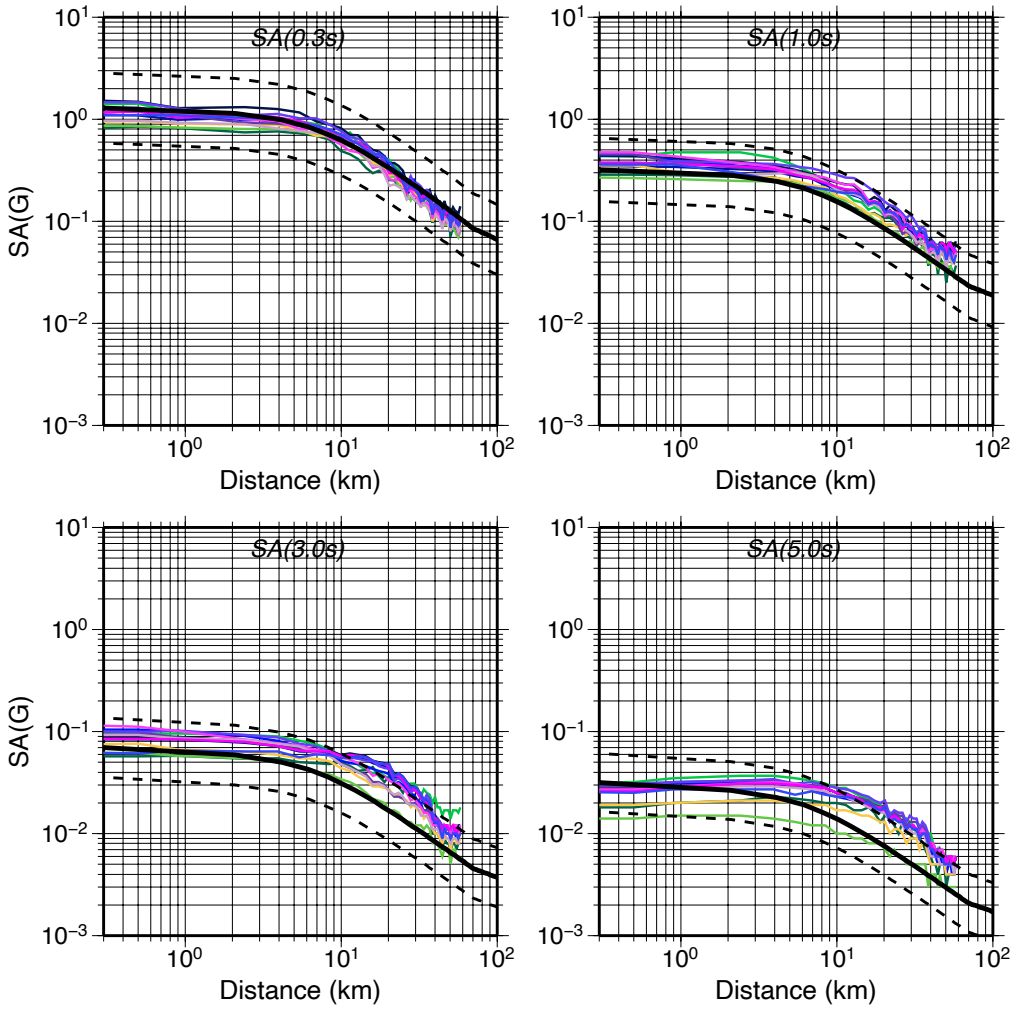

Figure 18. Near-fault ground motion saturation. Comparison of simulated (colored traces) and predicted RotD50 SA by Graizer's G-16v2 GMM **(**black traces). The colored traces correspond to synthetic ground motion computed with 10 rupture scenarios with different slip distributions.

Our simulation of ground motions from *Mw*6.5 earthquake rupture scenarios suggests that the near-fault saturation is a robust feature of the ground motion that does not depend on specific kinematic rupture characteristics. The simulated near-fault ground motion saturation supports findings in several studies that attribute the saturation to the radiation pattern effects combined with wave propagation effects (e.g. Chapman and Godbee, 2012; Baumann and Dalguer, 2014). It has been argued that for large earthquakes the saturation can be a result of several factors, including the local source radiation pattern, rupture directivity, low-velocity fault zone scattering (e.g., Li and

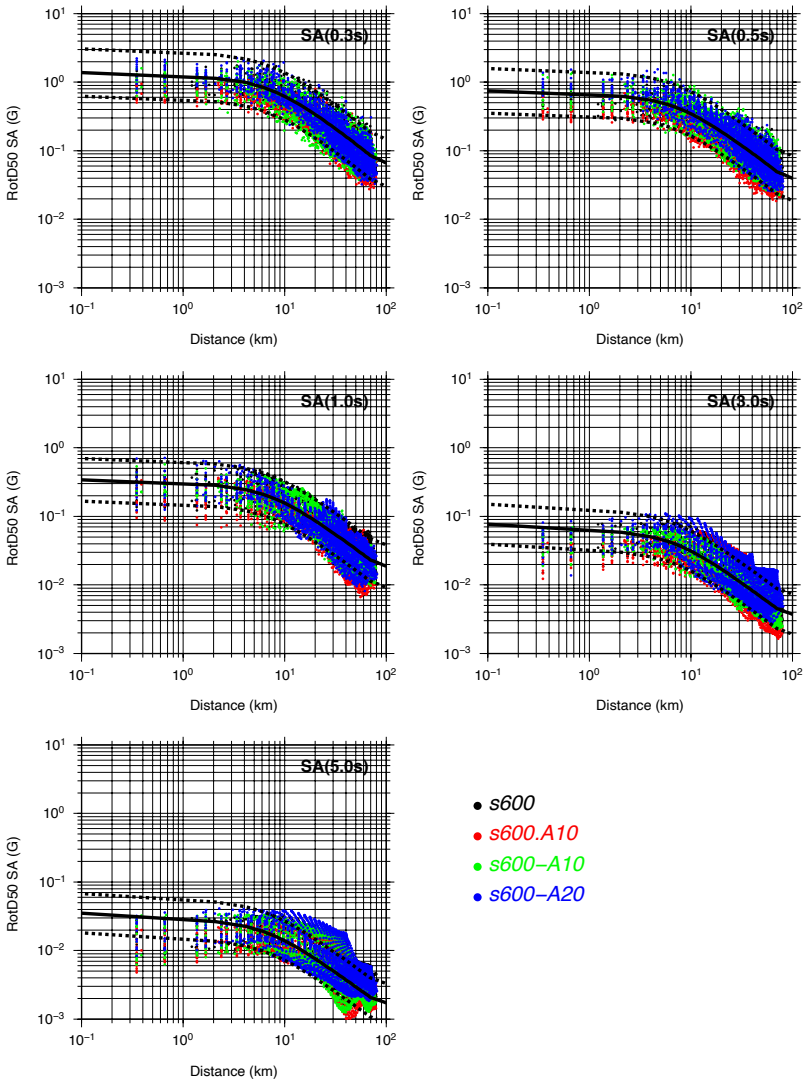

Figure 19. Effects of rupture area on simulated RotD50 SA for four different rupture areas: base slip distribution (black dots), rupture area increased by 10%(red dots), rupture area reduced by 10% (green dots) and rupture area reduced by 20% (blue dots). Black line shows Graizer's G-16v2 GMM.

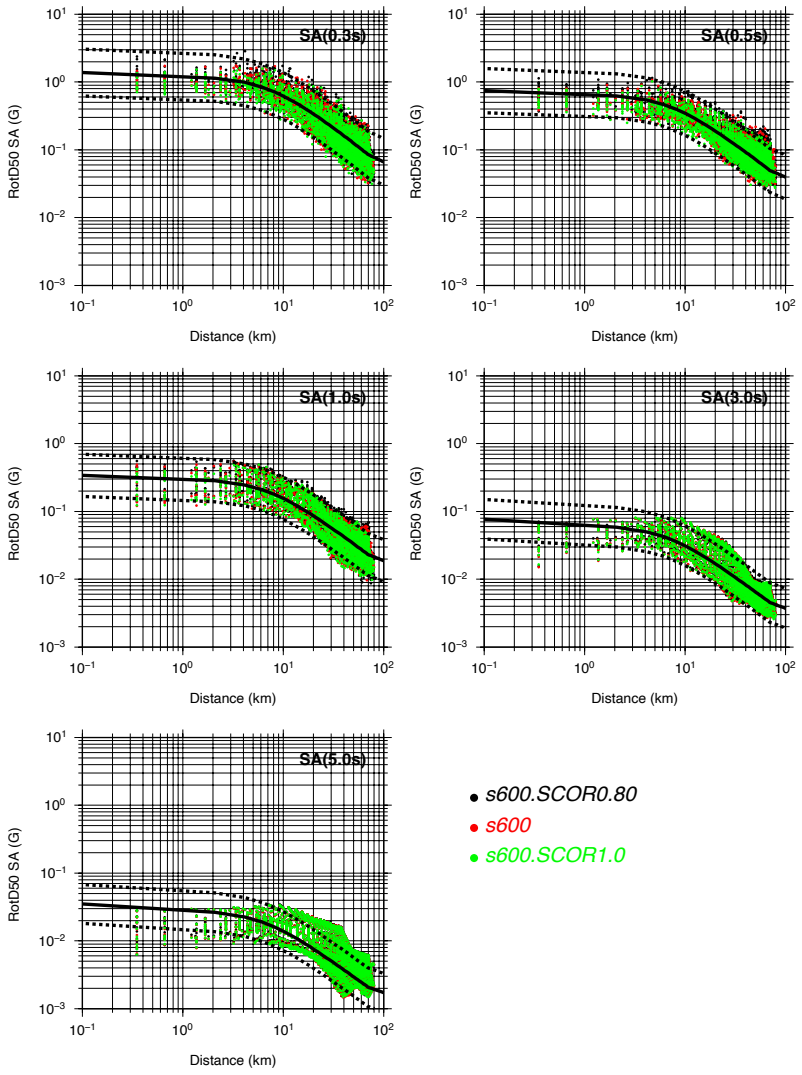

Figure 20. Effects of peak slip rate on simulated RotD50 SA obtained with different spatial slip rate roughness represented by different colors. Black line shows Graizer's G-16v2 GMM.

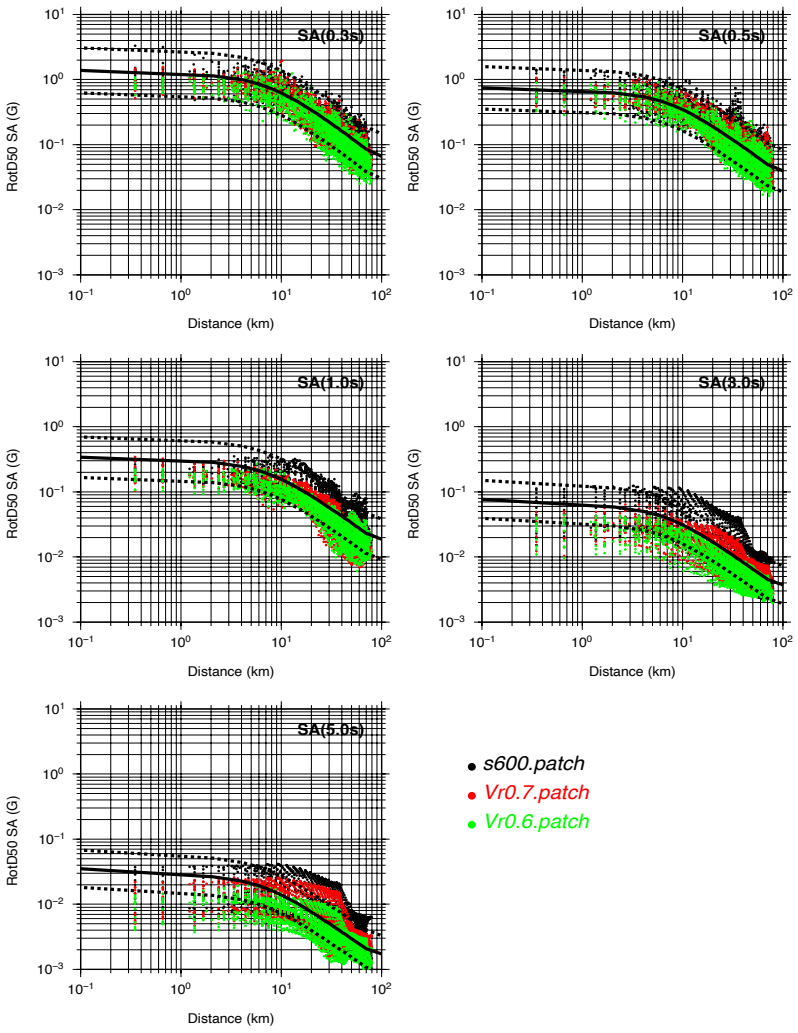

Figure 21. Effects of rupture velocity on simulated RotD50 SA obtained for three different average rupture velocities: Vr=0.8Vs (black dots), Vr=0.7Vs (red dots), Vr=0.6Vs (green dots). Black line shows Graizer's G-16v2 GMM.

Vidale, 1996), and nonlinear soil response. For long faults the oversaturation is a direct consequence of the definition of the source distance as closest distance from the fault plane. The closest distance to the fault does not necessary represent the distance from the most energetic part of the fault rupture. The so-called strong motion generation areas are often relatively deep, and in the case of large earthquakes they are concentrated in distributed small areas with high stress drop. Consequently, as shown by our simulations, their cumulative effect on ground motion time history is stronger at stations away from the

fault where the wave generated from these energetic parts of the fault are more coherent, as opposed to short fault-distance locations along the fault trace.

Our simulations of M6.5 thrust fault earthquakes indicates that the near-fault attenuation of the horizontal ground motion is significantly different from that of M6.5 strike-slip earthquakes. The simulated near-fault saturation is very week for the thrust fault. The ground motion gradually increases with decreasing fault distance. This trend is illustrated in figure 20 which shows the RotD50 SA as a function of distance, computed at different periods.

5.0 DIRECTVITY EFFECTS ON THE VARIABILITY OF NEAR-FAULT EARTHQUAKE GROUN DMOTION FOR STRIKES SLIP RUPTURES

We performed a series of simulations for moment magnitude, M_W, 6.5 strike-slip earthquakes with variable hypocenter location to investigate the impact of directivity on near-fault strong ground motion intensities. Ruptures were generated using the GP method including recent updates for hybrid ruptures with slip patches (Pitarka et al., 2022). For each slip distribution we considered five hypocenter locations. Ground motion intensities (GMI's) were measured and analyzed, specifically the peak ground acceleration (PGA), peak ground velocity (PGV), and RotD50 spectral accelerations at 0.3, 1 and 3 seconds. GMI's were highly variable in regions of forward and backward directivity aligned with the fault and less variable in areas normal to the fault. The standard deviation of GMI's from five ruptures of the same slip distribution can be as high as 0.6 natural logarithm units (nearly a factor of two) for sites aligned with the fault but are closer to 0.2 normal to the fault. The variability seen at sites aligned with the fault approaches the standard deviation (sigma) in median values from ground motion models (GMM's). This analysis demonstrates a breakdown of the ergodic assumption commonly used in GMM's and suggests that a path-dependent sigma may better represent expected GMI's for seismic hazard calculations.

Directivity is the azimuthal variation of radiated seismic energy due to rupture growth on an extended earthquake fault. It was observed in intermediate period teleseismic recordings. Early reports of inferred directivity in local strong motion records were made for California earthquakes such as the 1971 San Fernando, 1979 Coyote Lake and 1979 Imperial Valley earthquakes. Although interpretation of directivity may have been compromised by rupture complexity, path and site effects. Clear observations of directivity were reported by Boatwright and Boore (1982) from common recordings of the M_W 5.8 mainshock and M_W 5.5 aftershock of the January 1980 Livermore earthquakes. These events ruptured adjacent segments of the Greenville Fault with opposite directivity

and resulted in a factor of 10 variations in peak and root-mean square accelerations. There have been many studies to quantify the effects of directivity and incorporate them into ground motion models (Spudich et al.,2008,2013)

To investigate directivity, we ran SW4 simulations for a moment magnitude, M_W, 6.5 vertical strike-slip earthquake with a range of hypocenters and the Earth model fixed as described above. The fault dimensions were 26 km along strike and 8 km down dip. The rupture speed was fixed to 0.82 the shear wave speed. For the patch case we concentrated slip in the top center of the fault. Figure 22 shows the slip distributions for stochastic and patch cases and a single hypocenter. For the two slip distributions shown in Figure 22 we considered five (5) hypocenters: left, mid-left, center, mid-right and right right corresponding to geographic locations: southern, mid-southern, center, mid-north and north (shown in Figure 23). These hypocenter locations were -11, -6, 0, 6 and 11 km and at 6 km depth relative to the top center of the fault plane. A total of ten (10) SW4 simulations were run for the two slip distributions (stochastic and patch) and 5 hypocenters.

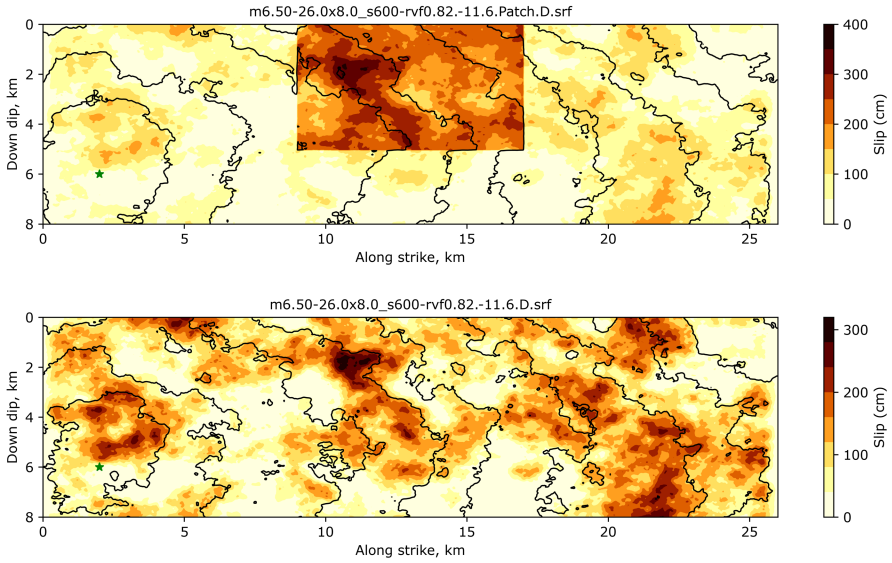

Figure 22. Earthquake ruptures models generated with the Graves and Pitarka methodology (Pitarka et al., 2022) considered in this study: (**top**) stochastic and (**bottom**) patch. Slip is plotted according to the color bar. The hypocenters are indicated by the green star and lines of constant rupture time (contour interval of 1s) are shown.

5.1 Analysis of Ground Motion Intensities

Time-histories were output for each simulation as HDF5 files. Ground motion intensities were measured for each rupture and site. Figure 24a shows example horizontal component velocity and acceleration ground motion time-histories at a site. Data were

saved and analyzed in MKS units. We then measured the RotD50 pseudo-acceleration response spectra with 5% damping for each site. Figure 24b shows the measured RotD50 spectrum for the waveforms in Figure 24a along with NGA-West2 (Goulet et al.,2021) ground motion model predictions. We also measured the geometric mean of the peak ground velocity and acceleration, PGV and PGA, respectively.

To investigate directivity effects, we plotted the ground motion intensities in map view. Figure 25 shows the PGV values in map view for the stochastic slip distribution and 5 hypocenters. Elevated values are seen in the forward directivity direction. Numerical simulations of earthquake ground motions such as the SW4 simulations considered here allow us to perform experiments that are possible in nature. For example, we can compute the ground motion intensities (GMI's) for the same slip distributions but with various hypocenters. We can then evaluate the common features and differences in the ground motions due to the different hypocenters considered. In this case we computed the mean, standard deviation and range of GMI's at each site. These can be visualized in map view for PGV and the stochastic slip distribution in Figure 26.

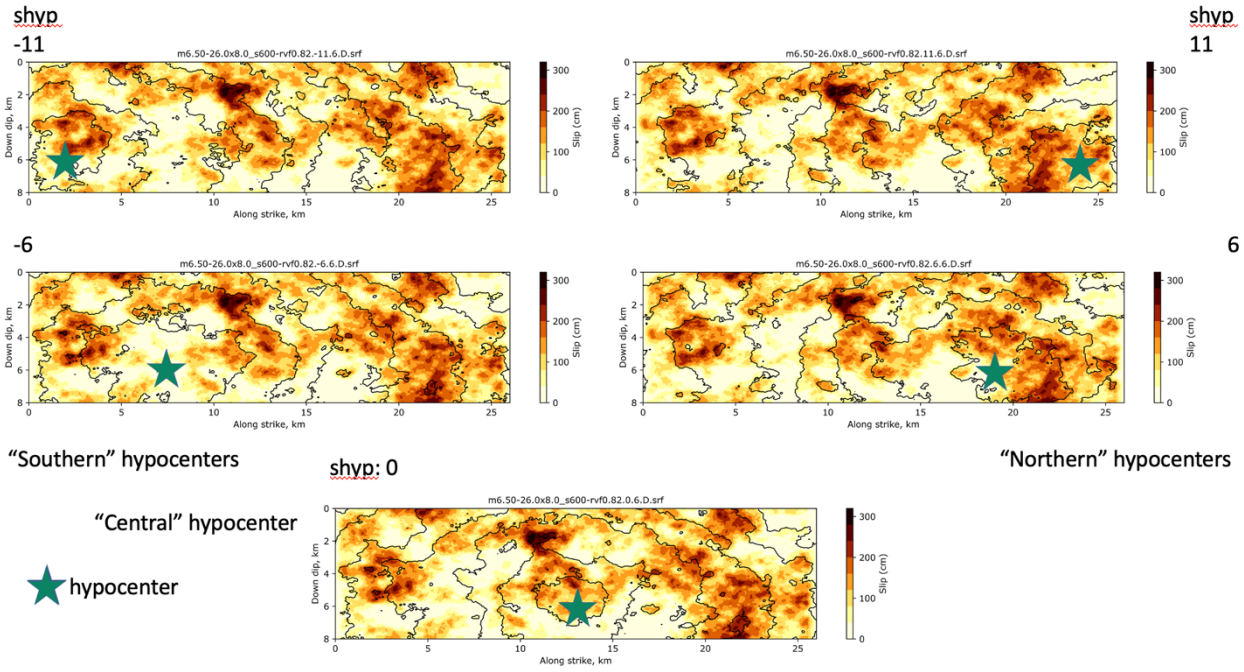

Figure 23. Earthquake rupture models for the stochastic slip distribution with the five (5) hypocenters considered.

Figure 26a shows the mean PGV for the five hypocenters with the expected "racetrack" pattern of PGV attenuating with Joyner-Boore distance away from the fault. Figure 26b shows the standard deviation of PGV and this shows a striking pattern of high values corresponding to high corresponding to low variability perpendicular to the fault. The

range of PGV values, defined as the natural logarithm of the ratio of the maximum to minimum values, is shown in Figure 26c. The spatial pattern of the range of PGV values tracks that of the standard deviation, but with larger values.

These maps show that a site off the ends of the fault can have about standard deviation of up to 0.6 log units or a factor of two while sites perpendicular to the fault have much lower variability with standard deviations of less than 0.2 log units. The variability off the ends of the fault (0.6 log units) is on par with the standard deviation of most ground motion models for typical GMI's. This suggests that variability in GMI's can be strongly influenced by directivity. The range of PGV values shows the PGV values can vary by about a factor of $e^{1.6}$ or about a factor of five.

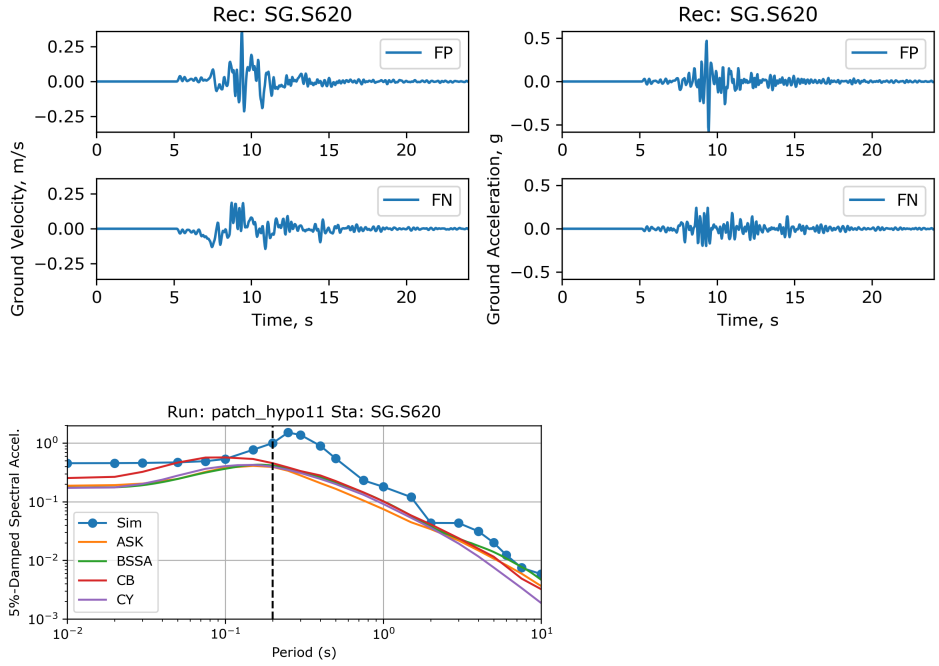

Figure 24. Example of simulated ground motions for the *Mw* 6.5 earthquake ruptures consider here: **(a)** horizontal component velocity (left) and acceleration (right) time-histories and **(b)** RotD50 pseudo-acceleration response spectrum for the waveforms in **(a)** along with NGA-West2 predictions.

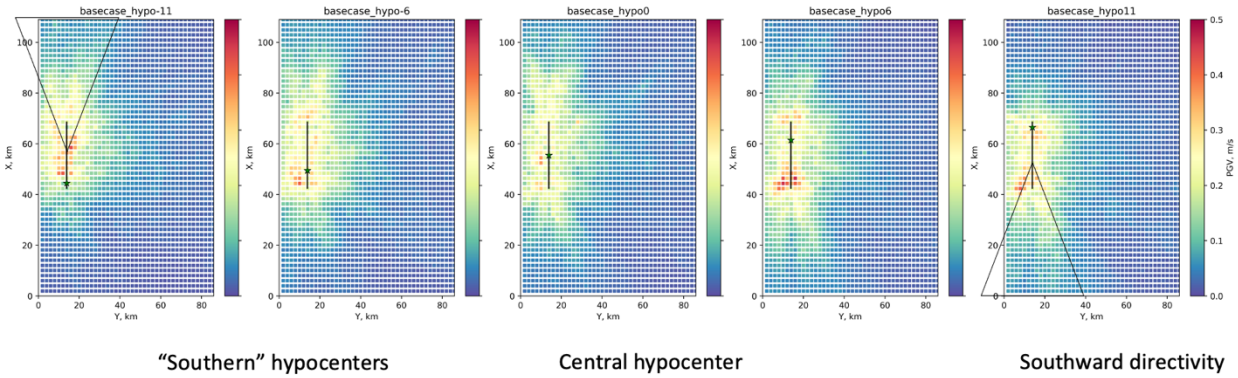

Figure 25. Map view peak ground velocity (PGV) for the stochastic slip distribution with 5 hypocenters indicated by the green stars. PGV is plotted according to the colorbar and shows elevated values in the forward directivity directions.

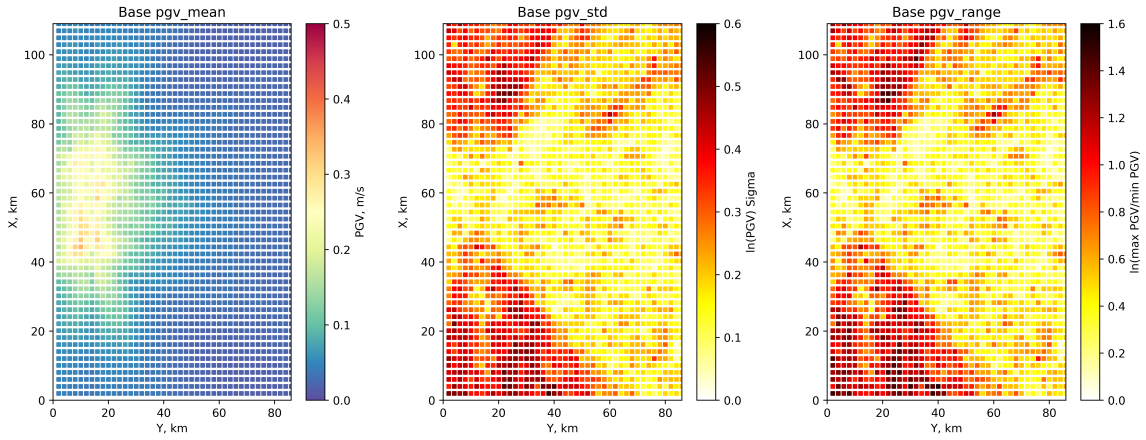

Figure 26. Map view of PGV aggregate intensities: (a, left) mean; (b, center) standard deviation; and (c, right) range.

6.0 CONCLUSIONS

Physics-based earthquake simulations are rapidly finding applications in seismic hazard assessment and structural engineering, supplementing the available earthquake record databases, and creating unprecedented opportunities for GMM improvements, site-specific seismic analysis and design of NPP structures. Due to advances in understanding of earthquake fault rupture processes and high-performance computing, the simulated earthquake ground motion incorporates significant realistic features on a

broad frequency range (e.g., McCallen et al., 2022, Rodgers et al., 2019). The main objective of this project was to provide technical capabilities for producing physics-based ground motion that can be used to constrain the GMMs for Stable Continental Regions (SCR) and Active Crustal Regions (ACR) at short distances and large magnitudes. Here we performed a feasibility study for M6.5 strike slip scenario earthquakes simulated using our Broad-Band Simulation Platform customized for earthquakes in the US Stable Continental Region.

In this study we build a regional 3D velocity model for CEUS by combining the Saikia's 1D velocity model with correlated stochastic perturbations. The hybrid model enhanced the performance of the waveform modeling on a broad frequency range. The proposed model was validated using comparisons of simulated and recorded data from two local earthquakes. The successful comparisons demonstrated the reliability of the 3D regional velocity model and the good performance of our deterministic simulation approach while emphasizing the importance of including small-scale variability in simulations of high-frequency wave scattering effects.

Additional validation analysis of the simulation platform, based on comparisons with different GMMs for a *Mw*6.5 earthquake in the CESUS region, resulted in a very good match between the simulated and empirical ground motion models. The successful validations against recorded earthquakes and empirical ground motion models justifies the use of synthetic waveforms in analysis of ground motion characteristics, such as within and between event variability and near-fault amplitude saturation.

The initial investigation of within-event and between-event ground motion variabilities for *Mw*6.5 scenario earthquakes on a strike-slip fault, suggests that they are strongly related to spatial slip and slip rate variations, average rupture velocity, rupture area and rupture initiation location. For certain scenarios we found that the ground motion variability observed at near-fault distances (< 5 km) also persists at longer distances.

Our simulation results suggests that the near-fault ground motion for an extended fault saturates at distances < 5km. Based on multiple realizations of the earthquake rupture, in which we varied different rupture model parameters, we found that the saturation is a robust feature of the ground motion that does not depend on specific kinematic rupture characteristics. The near-fault saturation has to do with the attenuation of waves propagating along the fault and local rupture radiation pattern that also contribute to stronger ground motion variation at such distances. The simulations support the hypothesis made by several GMM authors (e.g. Graizer et al., 2017;2018), that the saturation is a consequence of the wave propagation cumulative effect being stronger at locations away from the fault where the wave generated from the energetic parts of the fault are more coherent, as opposed to short faut-distance locations along the fault.

Our ground motion simulations for thrust-type earthquakes with surface rupture suggest that the near-fault saturation for this type of rupture is very week. Moreover, for thrust faults, the strength of the horizontal motion saturation with fault distance is period dependent. These results support the hypothesis which attributes the near-fault saturation to combined radiation pattern and wave propagation effects.

We used synthetic data computed for a large number of rupture scenarios to also analyze the near-fault ground motion variability due to rupture directivity effects. Our simulations were used to demonstrate that for a strike slip earthquake the ground motion at sites off the ends of the fault can have a standard deviation of up to 0.6 log units or a factor of two while the ground motion at sites perpendicular to the fault have much lower variability, with standard deviations of less than 0.2 log units. The variability off the ends of the fault (0.6 log units) is on par with the standard deviation of most ground motion models for typical GMI's. This suggests that variability in GMI's can also be strongly influenced by the rupture directivity.

Our 3D regional velocity model includes a realistic surface topography with higher elevations and roughness in the northern part of the model. The topography was extracted from the western North Carolina. Using simulated ground motions on a dense grid of stations we investigated potential topographic effects on ground motion amplitude. Overall, our analysis of topographic effects suggest that the local topography slightly amplifies (by ~30%) the ground motion amplitude in the simulated frequency range 1-3Hz. The effect of topography is pronounced in the surface and coda waves portions of the strong motion waveforms. Maps of simulated PGA and PGV indicate for a slight increase in amplitude in areas with pronounced surface topography. We concluded that because of the very high Vs in the shallow layers of our regional model the surface topography, in general, has minor effects in the simulated frequency range 0-5Hz.

In a second phase of this investigation, we plan to use our physics-based platform in computing ground motion from *Mw*7 and *Mw*7.5 earthquakes on a broad frequency range. The scenario-based synthetics will supplement ground motion data bases for short distances and large magnitude earthquakes in the CEUS region.

Acknowledgements

This work was funded by the U.S. Nuclear Regulatory Commission under contract 31310021S0002, and the work of A. Pitarka, A. Rodgers, and A. Aguiar was performed under the auspices of the U.S. Department of Energy by Lawrence Livermore National Laboratory under Contract DE-AC52-07NA27344. LLNL-TR-849902. Simulations were performed on the Quartz CPU platform and Lassen graphics processing unit accelerated

platform at LLNL, operated by Livermore Computing using a Computing Grand Challenge allocation.

7.0 REFERENCES

Baumann, C., and L. A. Dalguer (2014). Evaluating the compatibility of dynamic rupture-based synthetic ground motion with empirical ground-motion prediction equation, Bull. Seismol. Soc. Am. 104, no. 2, 634–652.

Boatwright J., D. Boore (1982). Analysis of the ground accelerations radiated by the 1980 Livermore valley earthquakes for directivity and dynamic source characteristics. Bull. Seismol. Soc. Am.,72,6,1843-1865.

Chapman, M. C., and R. W. Godbee (2012). Modeling geometrical spreading and the relative amplitudes of vertical and horizontal high- frequency ground motions in eastern North America, *Bull. Seismol. Soc. Am*. 102, no. 5, 1957–1975.

Graves, R. and A. Pitarka (2016). Kinematic Ground-Motion Simulations on Rough Faults Including Effects of 3D Stochastic Velocity Perturbations, *Bulletin of the Seismological Society of America,* **106**(5), 2136–2153, doi:10.1785/0120160088.

Graizer, V. (2016). Ground-Motion Prediction Equations for Central and Eastern North America. *Bull. Seism. Soc. Am*., **106**, 1600–1612.

Graizer, V. (2017). Alternative (G-16v2) Ground-Motion Prediction Equations for Central and Eastern North America. Bull. Seism. Soc. Am., **107**, 869-886.

Graizer, V. (2018). GK17 Ground-Motion Prediction Equation for Horizontal PGA and 5% Damped PSA from Shallow Crustal Continental Earthquakes. *Bull. Seism. Soc. Am*., **108**, 380-398.

Goulet, C. Y. Bozorgnia, G.M. Atkinson (2021). NGA-East Ground-Motion Characterization model part I: Summary of products and model development, Earthquake Spectra, https://doi.org/10.1177/87552930211018723.

Herrmann, R. B. (1995). Broadband seismology and small regional seismicnetworks, in Investigation of the New Madrid Seismic Zone, K. M.Shedlock and A. C. Johnston (Editors), U.S. Geol. Surv. Profess. *Pap. 1538.*

Li, Y. G., and J. E. Vidale (1996). Low-velocity fault-zone guided waves: Numerical investigations of trapping efficiency, *Bull. Seismol. Soc. Am*. 86, 371–378.

McCallen, D., N. A. Petersson, A. Rodgers, A. Pitarka, M. Miah, F. Petrone, B. Sjogreen, N. Abrahamson, H.Tang (2020), EQSIM – A Computational Framework for Fault-to-Structure Earthquake Simulations on Exascale Computers Part I: Computational Models and Workflow, *Earthquake Spectra*, https://doi.org/10.1177/8755293020970982

McCallen, D., F. Petrone, M. Miah, A. Pitarka, A. Rodgers, N. Abrahamson (2020), EQSIM – A Multidisciplinary Framework for Fault-to-Structure Earthquake Simulations on Exascale Computers Part II: Regional Simulations of Building Response , *Earthquake Spectra*, https://doi.org/10.1177/8755293020970980

Pitarka, A., and R. Mellors (2021), Using Dense Array Waveform Correlations to Build a Velocity Model With Stochastic Variability, Bull. Seismo. Soc. Am.,1–21, doi: 10.1785/0120200206.

Pitarka A**.,** R. Graves, K.Irikura, H. Miyake, and A. Rodgers (2017). Performance of Irikura Recipe Rupture Model Generator in Earthquake Ground Motion Simulations with Graves and Pitarka Hybrid Approach, *Pure and Applied Geophysics*, **174**(9), doi:10.1007/s00024-017-1504-3.

Pitarka, A., R. Graves, K. Irikura, K. Miyakoshi, C. Wu, H. Kawase, A. Rodgers, and D. McCallen (2022). Refinements to the Graves–Pitarka Kinematic Rupture Generator, Including a Dynamically Consistent Slip-Rate Function, Applied to the 2019 M_W 7.1 Ridgecrest Earthquake. Bull. Seism. Soc. Am, 112,(1):287-306. https://doi.org/10.1785/0120210138

Rodgers, A.J., A. Pitarka, R. Pankajakshan, B. Sjögreen, and N.A. Petersson (2020). Regional-Scale Three-Dimensional Ground Motion Simulations of Mw 7 Earthquakes on the Hayward Fault, Northern California Resolving Frequencies 0-10 Hz and Including Site Response Corrections, *Bull. Seismo. Soc. Am.*, (published online 8/11/2020), doi: 10.1785/0120200147.

Rodgers, A., A. Pitarka, N. A. Petersson, B. Sjogreen, D. McCallen and N. Abrahamson (2019). Broadband (0-5 Hz) fully deterministic three-dimensional ground motion simulations of a magnitude 7.0 Hayward Fault earthquake: comparison with empirical ground motion models and 3D path and site effects from source normalized intensities, Seismo. Res. Lett., https://doi.org/10.1785/0220180261.

Rodgers, A, A. Pitarka**,** A. Petersson, B. Sjogreen, D. McCallen (2018). Broadband (0-4 Hz) Ground Motions for a Magnitude 7.0 Hayward Fault Earthquake with 3D Structure and Topography, *Geophysical Research Letters*, doi:10.1002/2017gl076505.

Saikia, C. (1994). Modified frequency-wavenumber algorithm for regional seismograms using Filon's quadrature: modelling of L_g waves in eastern North America, *Geophysical Journal International*, Volume 118, Issue 1, July 1994, Pages 142–158, https://doi.org/10.1111/j.1365-246X.1994.tb04680.x

Somerville et al. (1997). Modifications of empirical strong motion attenuation relations to include the amplitude and duration effects of rupture directivity. *Seism. Res. Lett.,* 68(1):199-222.

Spudich P., and B. Chiu (2008) Directivity in NGA Earthquake Ground Motions: Analysis Using Isochrone Theory, *Earthquake Spectra*.

Spudich, P., Bayless, J. R., Baker, J. W., Chiou, B. S. J., Rowshandel, B., Shahi, S. K., & Somerville, P. (2013). Final Report of the NGA-West2 Directivity Working Group, PEER Report 2013-09. Pacific Earthquake Engineering Research Center, University of California, Berkeley, CA. https://peer.berkeley.edu/sites/default/files/webpeer-2013-09-paul_spudich_jeffrey_r._bayless_jack_w._baker_brian_s.j._chiou_badie_rowshandel.pdf

Taylor J., M. Celebi, A. Greer, E. Jampole, A. Masroor, S.Melton, D. Norton, N. Paul, E. Wilson, and Y. Xiao (2017). EERI Earthquake Reconnaissance Team Report: M5.0 Cushing Oklahoma USA Earthquake on November 7, 2016.

Presentations Related to the Project:

Pitarka, A, A. Rodgers, A. Aguiar, V. Graizer (2023). Physics-based Broadband Ground Motion Simulations of M6.5 Scenario Earthquakes in Central and Eastern US, including Surface Topography: Ground Motion Variability Related to Earthquake Rupture Characteristics, Oral presentation at the *Annual Meeting of the SSA, San Juan*, Puerto Rico, April 2023.